

Velocity-dependent phase shift in a light-pulse atom interferometer

Léo Morel,^{1,*} Zhibin Yao,¹ Pierre Cladé,¹ and Saïda Guellati-Khelifa^{1,2}

¹*Laboratoire Kastler Brossel, Sorbonne Université, CNRS,*

ENS-PSL University, Collège de France, 4 place Jussieu, 75005 Paris

²*Conservatoire National des Arts et Métiers, 292 rue Saint Martin, 75003 Paris, France*

Atom interferometry relies on the separation and recombination of atom wavepackets. When the two paths overlap perfectly at the end of the interferometer, the phase is insensitive to the atomic velocity distribution. Here, we show that, when the separation and recombination is performed using a Raman transition there is a displacement of the atomic wavepacket due to a phase shift during light pulses. Because of the variation of the laser intensity seen by the atoms, there is an imperfect cancellation of these displacements. The observation of a velocity-dependent phase shift on the interferometer is the signature of this effect, which has been modeled. Thanks to the signature we have identified, we are able to compensate for this effect by applying laser power ramps during the interferometer to mitigate intensity variations.

I. INTRODUCTION

Light-pulses used to perform two-photon Raman transitions or Bragg diffraction enable to coherently separate and recombine atomic wave functions [1, 2]. Based on such pulses, atom interferometers have been used in various applications such as the measurement of the Newtonian gravitational constant[3, 4], of the fine structure constant [5, 6], or have served to test the equivalence principle [7–10]. Achieving the accuracy required for these applications relies on careful designs. Most notably, the time sequence of the light pulses that operates the atom interferometer is always arranged in a symmetric way so that the two interfering atomic wavepackets overlap at the end. In this case, the initial velocity of the atoms does not affect the phase of the atom interferometer. This condition is similar to that of an optical interferometer working in white light, when the delay between the two arms is identical.

Usually, the computation of the phase includes only the phases imprinted by the lasers on the atoms that perform the transition [11]. Nevertheless, atoms remaining in the initial state undergo an additional phase shift that results in a displacement of the central position of the atomic wavepacket. The magnitude of this displacement depends on the laser intensity perceived by the atoms. If the atoms perceive a constant laser intensity over the interferometric sequence, this displacement is the same for both arms and thus the interferometer remains closed.

However, in experiments, the laser beams that drive the optical transitions are spatially finite with an intensity profile that is usually Gaussian. Moreover, the atoms that are interrogated are not at zero temperature and possess a transverse velocity (orthogonal to the beams propagation direction). Hence, the intensity that an atom perceives along the interferometric sequence varies: both the transverse velocity of the atoms and the intensity profile of the Raman laser beams restore sensitivity

to the longitudinal velocity distribution. The sensitivity of atom interferometers is usually enhanced by increasing their duration. However, in such a configuration the expansion of the atomic cloud is larger, therefore the bias associated with this effect compromises the gain in sensitivity. We evaluate the corresponding phase shift to a few tens of mrad, which does not affect the contrast of the interferometer.

The effect we report here has already been studied in [12]. Using the formalism of the sensitivity function, the authors investigated how this phase shift sets a limit to the symmetry of the $\pi/2 - \pi - \pi/2$ atom gravimeter. Notably, their work focused on the impact of this parasitic phase shift on the accuracy and long-term stability of the gravity measurement.

In this paper, we present a more general approach. We have theoretically modeled this phase shift for a Raman transition, which enables to evaluate its contribution in other interferometer geometries. We then study experimentally the behavior of this phase shift as a function of the atomic mean velocity and propose a method to mitigate its contribution to the total phase shift. We used the experimental setup designed to the measurement of h/m [5] where the atom interferometer is realized using Raman transitions and the ^{87}Rb atom cloud is produced in an optical molasses with a $1/e$ velocity distribution width of 2 cm/s ($T \approx 4 \mu\text{K}$).

Because of light shifts during Raman transitions, the variation of intensity during the interferometer also induces a related phase shift, which is coupled to the wavepacket displacements that we study here. In this paper, we compute a general formula that takes into account both effects. Furthermore, the method of compensation that we present also limits the impact of the light shifts.

The paper is organized as follows: we start by presenting a theoretical model to evaluate this displacement of the atomic wavepacket and to provide a general formula of the phase shift. Then, we present our experiment and the protocol we set up to observe this phenomenon. Finally, we show that we mitigate the related systematic bias by compensating for the variation of the laser power

* leo.morel@lkb.upmc.fr

ms), we find a displacement of 13 nm. This computation based on formula (7) allows us to compute the displacement for a narrow velocity distribution centered on the Raman resonance condition. In the following part, we generalize the treatment to other velocities.

III. FORMULATION OF THE EFFECT AS A PHASE SHIFT

A. Case $\delta_{LS} = 0$

In order to obtain a formula for any velocity, we calculate the phase shift that applies on the interferometer arm that is not diffracted during the Raman transition. We study the following quantity for state $|j\rangle$ ($j = 1, 2$):

$$\delta\phi = \arg(\langle j|U(\tau)|j\rangle / \langle j|U_0(\tau)|j\rangle), \quad (10)$$

which corresponds to the phase difference between the cases with and without coupling.

Combining equations (4) and (10), we obtain the following formula for the additional phase shift induced by the Raman coupling:

$$\delta\phi = \arctan\left(\frac{\delta'_D}{\sqrt{1+\delta_D'^2}} \tan\left(\frac{\theta\sqrt{1+\delta_D'^2}}{2}\right)\right) - \frac{\delta'_D\theta}{2}, \quad (11)$$

where $\theta = \Omega\tau$ is the pulse area and $\delta'_D = \delta_D/\Omega$ is the reduced Doppler detuning. If $\delta_D \rightarrow 0$, we find as expected that $\delta\phi \rightarrow 0$, *i.e.* the coupling does not induce an additional phase shift. On the other hand, for $\delta_D \gg \Omega$, we develop equation (11) and obtain $\delta\phi \approx \Omega^2\tau/(4\delta_D)$ which corresponds to the prediction of the first order perturbation theory.

We present the behavior of the intermediate case in figure (2) where the phase shift is plotted with respect to δ'_D . We notice that the width of the dispersion figure scales inversely with the pulse area. This can be interpreted as an illustration of the Heisenberg principle: as the pulse duration increases, its resonance frequency gets defined with a better precision.

Now that we have treated the case of a single pulse, we can study the case of an interferometric sequence. To this end we will continue considering the Ramsey-Bordé sequence presented in figure (1). The perturbation phase shift $\delta\phi$ is now given only by the arctan term of equation (11) because the Doppler terms compensate each other.

The phase shift only applies on the wavepacket that remained in the same internal state during the Raman transition. We outline that the phase shift is the same in magnitude for the two states but changes sign.

Moreover, we write the total phase shift at the output of the interferometer $\Phi^{(B)} - \Phi^{(A)}$ where (A) and (B) are the arms displayed on figure (1). We obtain that the contribution of this parasitic effect writes:

$$\Delta\Phi = \delta\phi_4 + \delta\phi_3 - \delta\phi_2 - \delta\phi_1 \quad (12)$$

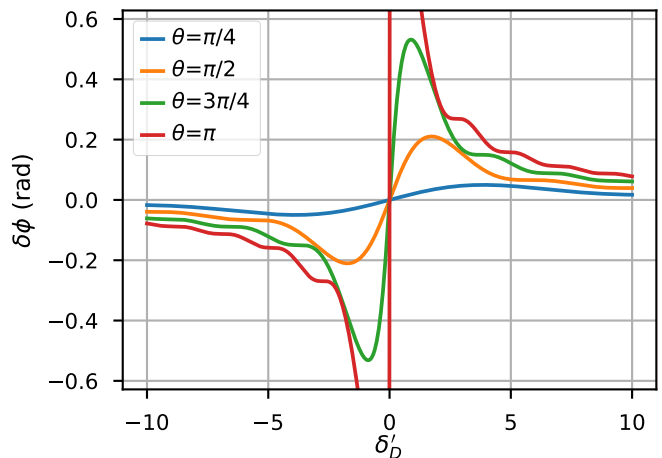


FIG. 2. Plot of equation (11). Single-pulse phase shift with respect to δ'_D for different pulse areas.

The sign of the contribution is the same for the two pulses of a single pair, hence leads to an important non uniform phase shift that depends on the longitudinal velocity of the atoms. Besides, the effect is exalted by increasing the total duration of the interferometer which is consistent with the T scaling obtained in equation (9). More precisely, using the approximation of equation (8), the formula (12) can be linearized with respect to the parameter βT . We obtain:

$$\Delta\Phi = \beta T f_D(\delta'_D, \theta), \quad (13)$$

where the function f_D is plotted in figure (3) and evaluates to:

$$f_D(\delta'_D, \theta) = \frac{2\delta'_D \left(\sin\left(\frac{\theta\sqrt{1+\delta_D'^2}}{2}\right) - \theta\sqrt{1+\delta_D'^2} \right)}{\sqrt{1+\delta_D'^2} \left(2\delta_D'^2 + \cos\left(\frac{\theta\sqrt{1+\delta_D'^2}}{2}\right) + 1 \right)}. \quad (14)$$

This function behaves like a dispersion relation and displays its maximal sensitivity to δ'_D around zero, which corresponds to the usual operating conditions for interferometers. In order to reduce the sensitivity of the output phase of the interferometers to this effect, we act on the parameter β and observe a reduction of the amplitude of the dispersion curve.

B. Case $\delta_{LS} \neq 0$

We now move to the case where the coupling induces an additional detuning because of a differential light shift $\delta_{LS} \neq 0$. Equation (11) is modified and becomes:

$$\delta\phi = \arctan\left(\frac{\delta'}{\sqrt{1+\delta'^2}} \tan\left(\frac{\theta\sqrt{1+\delta'^2}}{2}\right)\right) - \frac{\delta'\theta}{2}, \quad (15)$$

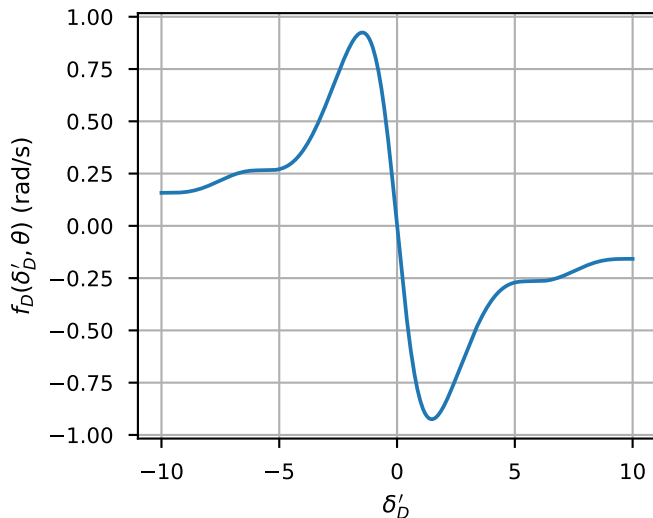


FIG. 3. Plot of the function $f_D(\delta'_D, \theta)$ (equation (14)) for a Ramsey-Bordé interferometer with pulse area $\theta = \pi/2$.

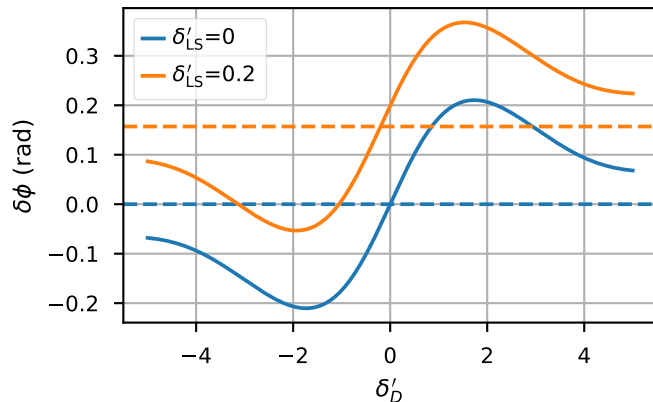


FIG. 4. Single-pulse phase shift (equation (15)) with respect to δ'_D for a $\pi/2$ pulse and different light shift intensities.

where $\delta'_{LS} = \delta_{LS}/\Omega$ and $\delta' = \delta'_D + \delta'_{LS}$ is the total reduced detuning. We represent in figure (4) this equation with respect to δ'_D , for different δ'_{LS} and for a pulse area of $\pi/2$. We observe both a vertical and horizontal displacement of the dispersion curve. Indeed, the differential light shifts both modify the accumulated phase between the two states and moves the resonance condition.

The question of the effects of level shifts induced by the coupling lasers has been addressed in the literature by analyzing a single pulse [16], or globally using the sensitivity function of an interferometer [17]. Using formula (15) in the limit of small differential light shift ($\delta'_{LS} \ll 1$), we find that the phase shift for a single $\pi/2$ pulse amounts to $\delta\phi = \delta'_{LS}$ which is used in the above references. Our formula is valid beyond the limit of small shifts and also takes into account the effect of the Doppler shift.

If the differential light shift δ_{LS} is constant during the interferometer, the phase shifts that it induces are cancelled. However, δ_{LS} is proportional to the lasers inten-

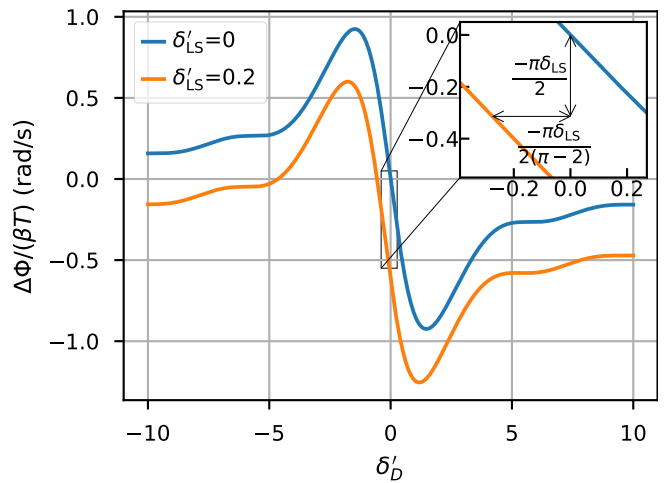


FIG. 5. Effect on a Ramsey-Bordé interferometer in the presence of differential light shift δ_{LS} during the light pulse. Inset: horizontal and vertical displacement of the curve for $\delta'_{LS} \ll 1$.

sity like the Rabi frequency Ω . Thus δ_{LS} varies and for the computations, we assume that it varies linearly with the same rate β . As a consequence, the dispersion curve of figure (3) is modified. In particular, for $\delta_{LS} \ll \Omega$ it is displaced both horizontally and vertically similarly to the single-pulse case (figure (4)). We display these displacements of the curve in figure (5) and obtain that they write $-\pi\delta'_{LS}/2$ vertically and $-\pi\delta'_{LS}/(2(\pi-2))$ horizontally, if the interferometer pulses are $\pi/2$.

However, even with the presence of light shift, the amplitude of the dispersion curve remains proportional to the parameter β . We have developed an experimental method to reduce this parameter, based on the measurement of the dispersion curves. We present this protocol in section V.

IV. EXPERIMENTAL SETUP

The design of our vacuum chamber is shown in figure (6). In the lower area, we produce cold samples of ^{87}Rb atoms using conventional techniques (optical molasses and three-dimensional magneto-optical-trap). The atoms are cooled down to $\approx 4 \mu\text{K}$. Upon release, the size of the atomic cloud ($1/e^2$ radius) is $500 \mu\text{m}$. The ground state of ^{87}Rb has two hyperfine levels $|F=1\rangle$ and $|F=2\rangle$.

The interferometry sequence takes place in a 70 cm long tube where the magnetic field is controlled within a few percent. To transport atoms to the interferometry area, we apply a Bloch Oscillations (BOs) pulse [18, 19] which transfers to the atoms 1300 atomic recoils upwards. The cloud then reaches the interferometry area within 60 ms. We then use a second 300 BOs pulse (600 atomic recoils) downwards 100 ms after the first pulse to control the trajectory of the atomic cloud. We point out that the timing and number of BOs parameters of the second

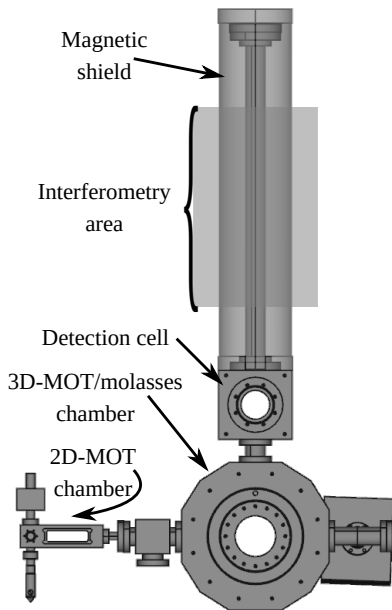


FIG. 6. Schematic of the vacuum cell.

pulse allows us to control precisely this trajectory, and we refer to this technique as an atom elevator[20].

The preparation of the internal state is performed during the atom elevator as follows: at the output of the optical molasses stage, the atoms are in $|F = 2\rangle$ (a short repump pulse removes all atoms from $|F = 1\rangle$) distributed among the five Zeeman sublevels of this hyperfine state. We apply a counterpropagating (Doppler sensitive) Raman π -pulse set to be resonant with the $|F = 2, m_F = 0\rangle \rightarrow |F = 1, m_F = 0\rangle$ transition at the center of the cloud velocity distribution. The Raman lasers are phase-locked, and their frequency difference and relative phase are controlled using a radiofrequency generator based on a RedPitaya FPGA device [21]. A blow-away pulse, resonant with the $|F = 2\rangle \rightarrow |F' = 3\rangle$ optical transition, removes atoms that did not perform the Raman transition. The atoms are then placed back to $|F = 2, m_F = 0\rangle$ with a second π Raman pulse. We control the width of the selected velocity class through the duration of the first Raman pulse, maintaining the $\Omega\tau = \pi$ condition. The second Raman π pulse is set at minimal duration, using the maximum available laser power, in order to transfer back all the atoms selected by the first pulse.

In our setup, the waist of the Raman beams is 4.9 mm, the typical maximum intensity is 130 mW/cm² and the duration of a π pulse is at least 60 μ s which corresponds to a Rabi frequency of 16.6 kHz. The Raman lasers are blue-detuned with respect to the one-photon transition by a large amount (≈ 60 GHz). In this paper, we focus on the study of the effect on a single interferometer. For precision measurements, we compensate parasitic phase shifts using the k-reversal technique [16, 20].

After this preparation stage, we apply the interferometric sequence. A schematic of the total sequence is

presented in figure (7) which represents the interferometer used to exhibit the effect (see section V).

The atomic state at the end of the interferometer is read by the detection setup placed in-between the optical molasses cell and the interferometry area. The free-falling atoms reach a system of resonant light sheets that detects separately atoms in $|F = 2\rangle$ and atoms in $|F = 1\rangle$ through a time-of-flight technique. We then estimate the proportion of atoms in each state by collecting the fluorescence the atoms emit as they cross the sheets onto large-area photodiodes.

V. RESULTS

In order to exhibit the effect, we implemented a Ramsey-Bordé interferometer with $T_R = 10$ ms and $T = 70$ ms. The complete sequence is represented in figure (7) with the exception of the third Bloch Oscillations pulse, not implemented at this stage.

Treating the Ramsey-Bordé interferometer at first approximation, the phase difference at the output of the interferometer between its two arms is proportional to the velocity acquired by the atoms between the first and third Raman interferometer pulses. The phase shift presented in section III acts as a perturbation of the differential velocity sensor signal.

In equation (15), both Ω and δ_{LS} depend on the cloud expansion and are difficult parameters to control over the interferometer. However, the parameter δ_D can be controlled by changing the frequency difference between the Raman lasers at the velocity-selection stage. Changing this parameter amounts to varying the mean Doppler detuning $\langle\delta_D\rangle$ of the atomic cloud.

The top part of figure (8) outlines the details of the technique. We scan $\langle\delta_D\rangle$ (dashed lines) without changing the Raman lasers frequency for the interferometer (black dotted line). The effective velocity distribution that contributes to the output of the interferometer (solid lines) is then slightly different from the initial distribution because of the interferometer pulse envelope.

We scan the phase of the last Raman pulse with 50 points equally distributed on a 2π interval, and estimate the position of the center of the fringe (phase shift) with a sinusoidal fit. This result is plotted on the bottom part of figure (8) for $\langle\delta_D\rangle = 0$ and 6 kHz. Because of the large detuning at $\langle\delta_D\rangle = 6$ kHz, the contrast of the fringe is reduced by $\approx 40\%$.

Using such a method, we obtain the phase at the output of the interferometer with a typical precision of 10 mrad. In figure (9), we plot the result of this measurement performed in the interval $[-6, 7]$ kHz with a step of 1 kHz. The measurement was repeated three times for each value of $\langle\delta_D\rangle$. The Rabi frequency of the interferometer pulses was 4.8 kHz.

The results are consistent with the prediction of figure (3). In particular, we observe that the zero of the curve is slightly shifted because of the light shift.

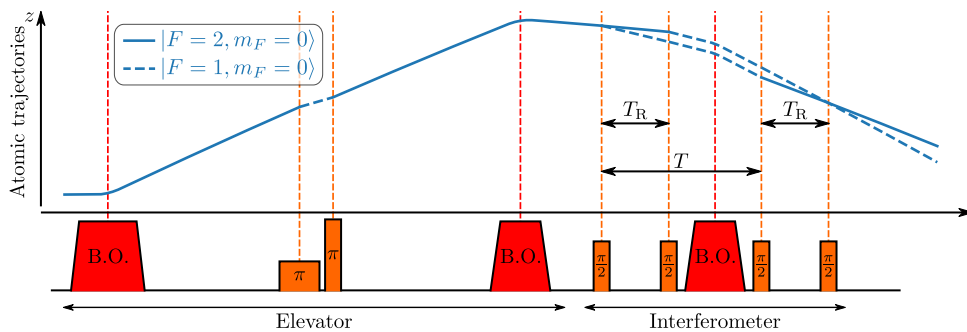


FIG. 7. Experimental sequence to observe the dependence of the interferometer output with respect to the atoms initial velocity $\langle \delta_D \rangle$. Left: elevator sequence based on Bloch Oscillations, with the velocity and internal state selection based on two counterpropagating Raman π pulses. Right: Ramsey-Bordé interferometer sequence. Blue line: Atom trajectory during an experimental sequence. Yellow lines: Raman pulses. Red areas: Bloch Oscillations pulses. The third Bloch Oscillations pulse, in the interferometer, is used to measure h/m .

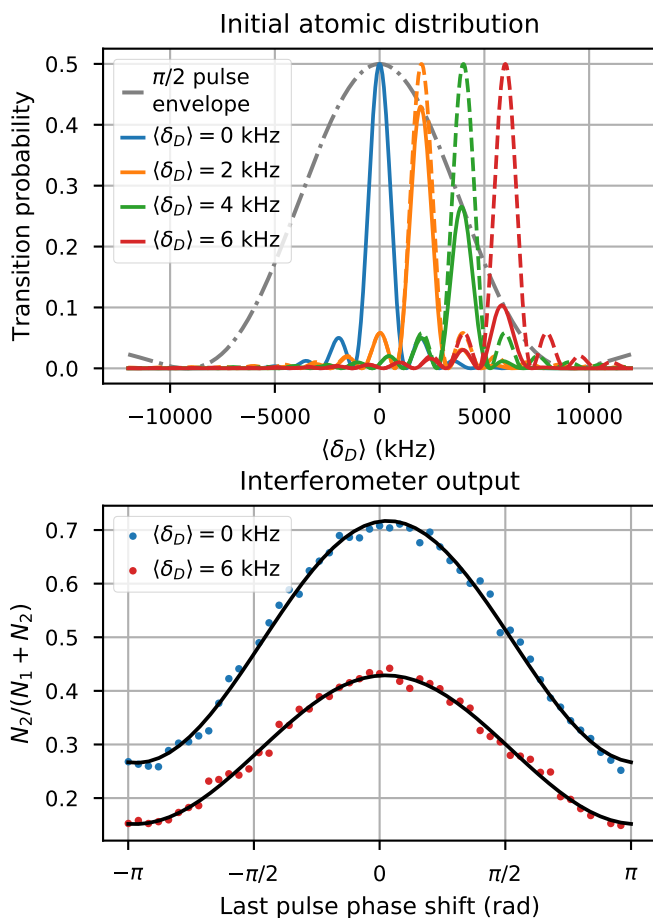


FIG. 8. Top: velocity distribution at the beginning of the interferometer. Gray dotted line: first $\pi/2$ envelope. Dashed line: velocity distribution before the first pulse for different setpoints of the velocity selection stage. Solid lines: velocity distribution after the first pulse. Bottom: proportion of atoms in $|F=2\rangle$ at the output of the interferometer with respect to the phase of the last $\pi/2$ pulse for two mean Doppler detunings.

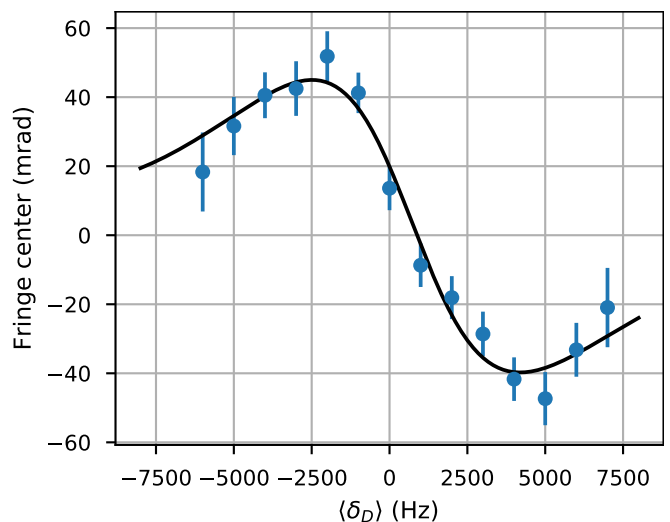


FIG. 9. Plot of the fringe center with respect to the mean Doppler detuning of the atomic cloud. The origin of the vertical axis is set to the average value of the dataset for visibility. Blue points: experimental data. Black line: fit obtained using equation (12).

The amplitude of the phase shift (≈ 80 mrad) is important compared to the aimed accuracy of this atom interferometer. For instance, the required precision for the measurement of h/m at the level of 0.1 ppb stands below the mrad level. Moreover, this effect depends on the longitudinal velocity of the atoms so that a careful estimation requires precise knowledge of the velocity distribution. However, even if one implements a control of the atomic velocity distribution, correlations between the atomic velocities and the efficiency of the detection system make a more accurate evaluation of this effect challenging [22]. Hence, we developed an experimental method to reduce the effect.

Because the parasitic phase shift is induced by the variation of perceived power, we increase the power of the Raman lasers, linearly with time, during the interferometer.

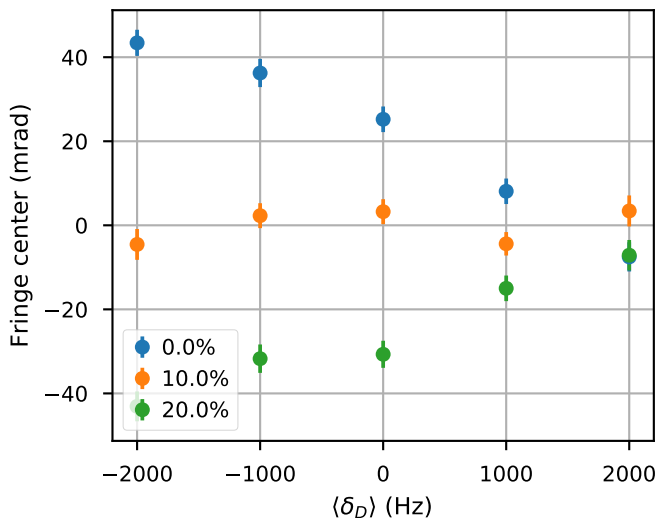


FIG. 10. Fringe center of the interferometer with respect to the mean Doppler detuning of the atomic cloud for variations of the laser power between the first and the last pulse. For this study, the Rabi frequency was 8 kHz. The origin of the vertical axis is set to the average value of the dataset for visibility.

We chose to apply a linear ramp because in our experiment the interferometry sequence begins about 170 ms after the release from the optical molasses phase: the transverse position of the atoms depends only on their velocity and we expect a quasi-linear variation of the average intensity perceived by the cloud with time.

The idea of the technique is to apply different laser power ramps on the Raman lasers, and scan the mean Doppler detuning of the atomic distribution at the input of the interferometer. As the perceived intensity is made more homogeneous for all the interferometer pulses, the dependency of the output phase with the Doppler shift is reduced. In particular, if the Rabi frequency Ω and the differential light shift δ_{LS} are the same for the four pulses, the phase shift of equation (15) is constant and is cancelled according to equation (12).

For the measurement of h/m , we insert in-between the Ramsey sequence a pulse of 500 BOs and measure the velocity the atoms acquired [5]. BOs is an adiabatic process whose survival probability (*i.e.* the probability to absorb two atomic recoils) depends sharply on the intensity and can be modeled by a step function [23]: atoms that perceive an intensity below a given threshold do not perform the BO and atoms above perform it. Thus, the BOs pulse performs a transverse selection of the atoms as those at the edge of the beams are not accelerated. The effective transverse velocity distribution that contributes to the interferometer signal depends on this BO pulse.

Hence, we performed the study with the BO pulse, *i.e.* in the condition of the measurement of h/m for different Raman power ramps: no power ramp and linear ramps that correspond to a power increase of 10% and 20% from the first to the last pulse of the interferometer. The result

of this study is displayed in figure (10). We observe that for the largest power ramp, the sign of the dependency of the phase with the mean Doppler detuning is changed, which means that the average intensity perceived by the atomic cloud increases along the interferometer instead of decreasing.

Finally for a 10% increase of the power at the last pulse, the effect is almost cancelled. We do not observe a perfect cancellation because the method of the power ramps is based on reducing the variation of the average intensity perceived by the atoms. Even with this power ramp, the atoms with zero transverse velocity perceive an increasing intensity along the interferometer and the atoms with the largest transverse velocity still perceive a decreasing intensity but with a smaller amplitude than without the power ramp.

Because of this limitation, we estimate that we reduced the sensitivity of the interferometer to the initial velocity distribution by 80%, which corresponds to the reduction of the amplitude of the curves displayed on figure (10).

These measurements outline that the sensitivity of the interferometer to the velocity distribution originates from the laser intensity variation of the Raman pulses. They also show that it is possible to reduce the sensitivity by applying an adequate power ramp. We highlight the fact that our method does not require *a priori* information on the velocity distribution of the atoms and that the power ramp is experimentally calibrated.

VI. CONCLUSION

In this paper, we have shown that during a Raman transition, the wavepacket that remains in the initial state undergoes a displacement. Because of variations of the Rabi frequency of the pulses, this displacement is not cancelled at the output of the interferometer which induces a sensitivity to the initial velocity distribution. By measuring the phase of the interferometer with respect to the initial velocity, we identify the dispersive signature of this effect. We have obtained an analytical formula of the phase of the interferometer that corroborates experimental observations. These general formulas can be adapted to any interferometer geometries based on Raman transitions.

The dispersive behavior as a function of the initial velocity is crucial to experimentally compensate the variation of the laser intensity perceived by the atoms during the interferometer. This protocol can be applied on particular interferometer configurations such as the one we use for the measurement of h/m .

Although we focused our treatment on Raman transitions, the model we have developed in this paper for velocity-dependent phase shift could be adapted to Bragg diffraction. We also believe that this effect should be accurately evaluated in experiments aiming at testing the equivalence principle with dual-species interferometer [7, 8, 10, 24, 25] and our approach would help for

seeking for a signature enabling a better compensation

of the systematic bias resulting from the variation of the laser intensity during the light-pulse sequence.

-
- [1] M. Kasevich and S. Chu, *Physical Review Letters* **67**, 181 (1991).
- [2] D. M. Giltner, R. W. McGowan, and S. A. Lee, *Physical Review Letters* **75**, 2638 (1995).
- [3] J. B. Fixler, G. T. Foster, J. M. McGuirk, and M. A. Kasevich, *Science* **315**, 74 (2007).
- [4] G. Rosi, F. Sorrentino, L. Cacciapuoti, M. Prevedelli, and G. M. Tino, *Nature* **510**, 518 (2014).
- [5] R. Bouchendira, P. Cladé, S. Guellati-Khélifa, F. Nez, and F. Biraben, *Physical Review Letters* **106**, 080801 (2011).
- [6] R. H. Parker, C. Yu, W. Zhong, B. Estey, and H. Müller, *Science* **360**, 191 (2018).
- [7] S. Dimopoulos, P. W. Graham, J. M. Hogan, and M. A. Kasevich, *Physical Review Letters* **98**, 111102 (2007).
- [8] D. Schlippert, J. Hartwig, H. Albers, L. L. Richardson, C. Schubert, A. Roura, W. P. Schleich, W. Ertmer, and E. M. Rasel, *Physical Review Letters* **112**, 203002 (2014).
- [9] B. Barrett, L. Antoni-Micollier, L. Chichet, B. Battelier, P.-A. Gominet, A. Bertoldi, P. Bouyer, and A. Landragin, *New Journal of Physics* **17**, 085010 (2015).
- [10] G. Rosi, G. D’Amico, L. Cacciapuoti, F. Sorrentino, M. Prevedelli, M. Zych, C. Brukner, and G. M. Tino, *Nature Communications* **8**, 15529 (2017).
- [11] P. Storey and C. Cohen-Tannoudji, *Journal de Physique II* **4**, 1999 (1994).
- [12] P. Gillot, B. Cheng, S. Merlet, and F. Pereira Dos Santos, *Physical Review A* **93**, 013609 (2016).
- [13] C. Bordé, *Physics Letters A* **140**, 10 (1989).
- [14] K. Moler, D. S. Weiss, M. Kasevich, and S. Chu, *Physical Review A* **45**, 342 (1992).
- [15] R. Jannin, P. Cladé, and S. Guellati-Khélifa, *Physical Review A* **92**, 013616 (2015).
- [16] A. Peters, K. Y. Chung, and S. Chu, *Metrologia* **38**, 25 (2001).
- [17] A. Gauguier, T. E. Mehlstäubler, T. Lévêque, J. Le Gouët, W. Chaibi, B. Canuel, A. Clairon, F. P. Dos Santos, and A. Landragin, *Physical Review A* **78**, 043615 (2008).
- [18] M. B. Dahan, E. Peik, J. Reichel, Y. Castin, and C. Salomon, *Physical Review Letters* **76**, 4 (1996).
- [19] S. R. Wilkinson, C. F. Bharucha, K. W. Madison, Q. Niu, and M. G. Raizen, *Physical Review Letters* **76**, 4512 (1996).
- [20] P. Cladé, E. de Mirandes, M. Cadoret, S. Guellati-Khélifa, C. Schwob, F. Nez, L. Julien, and F. Biraben, *Physical Review A* **74**, 052109 (2006).
- [21] P. Cladé, M. Andia, and S. Guellati-Khélifa, *Physical Review A* **95**, 063604 (2017).
- [22] T. Farah, P. Gillot, B. Cheng, A. Landragin, S. Merlet, and F. Pereira Dos Santos, *Physical Review A* **90**, 023606 (2014).
- [23] S. Bade, L. Djadaojee, M. Andia, P. Cladé, and S. Guellati-Khélifa, *Physical Review Letters* **121**, 073603 (2018).
- [24] A. Bonnin, N. Zahzam, Y. Bidet, and A. Bresson, *Phys. Rev. A* **88**, 043615 (2013).
- [25] P. Asenbaum, C. Overstreet, M. Kim, J. Curti, and M. A. Kasevich, “Atom-interferometric test of the equivalence principle at the 10^{-12} level,” (2020), arXiv:2005.11624 [physics.atom-ph].